ACS Energy LETTERS

http://pubs.acs.org/journal/aelccp

LETTER

Optical Properties of Lead-Free Double Perovskites by Ab Initio Excited-State Methods

Maurizia Palummo,* Eduardo Berrios,* Daniele Varsano,* and Giacomo Giorgi*

Cite This: *ACS Energy Lett.* 2020, 5, 457−463

Read Online

ACCESS | Metrics & More | Article Recommendations | Supporting Information

ABSTRACT: We discuss the nature of the optical excitations of $Cs_2AgBiBr_6$, the archetypal compound of lead-free double perovskites. Such quaternary material shows an indirect electronic band gap with a broad optical absorption spectrum above 2 eV. By means of ab initio excited-state methods we show that the first absorption peak is due to a bound direct exciton (near the X point of the Brillouin zone), while the photoluminescence spectrum is explained in terms of phonon-assisted radiative recombination of indirect-bound excitons with transferred momenta along the L−X and Γ−X directions. To address the role of metal and halide atoms on the electronic and optical properties of this materials class, we investigate two additional ternary double perovskites, i.e., $Cs_2In_2X_6$ (X = F, Br). On the basis of the accurate determination of the absorption coefficients and minimum gaps, we estimate the spectroscopic limited maximum efficiency of solar cells based on such compounds, providing relevant information for their application in photovoltaics.

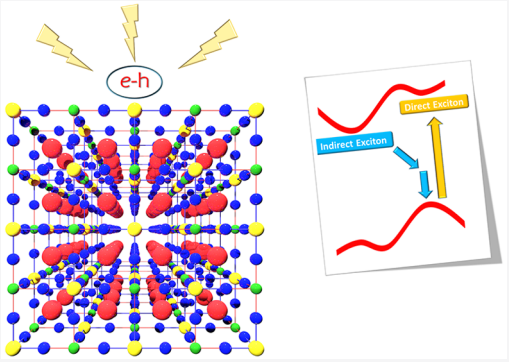

Bulk hybrid organic inorganic halide perovskites (OIHPs) and derived systems have completely changed the scenario of modern, cheap, photovoltaics (PV),[1−7] as testified by the huge conversion efficiencies (PCEs) reached by the perovskite solar cells (PSCs) that nowadays pass 23%.[8] Despite the so high PCEs reached by PSCs based on the archetypal compound $MAPbX_3$ (MA = $CH_3NH_3^+$, methylammonium; X = halide) as a light harvester, there remain issues mainly related to device stability and toxicity. For the former, the dimensionality reduction (3D → 2D, via the partial/total replacement of MA with longer-chain, hydrophobic, aliphatic (BA = butylammonium) or aromatic (PEA = phenethylammonium) organic cations), at the price of reduced PCEs, seems to be one of the best directions to follow.[9−12] The replacement of the organic moiety with other metallic ions (Cs) that actually recover the OIHP parental compounds, i.e., $CsPbX_3$,[13] has been also investigated as a possible strategy to improve the device stability. For the environmental issue, the replacement of Pb with other more ecofriendly elements[14] has been a subject of intense research since the dawn of this new PV technology. The so-called double perovskites where Pb(II) pairs are aliovalently replaced by two metals, one in the +1 and the other in the +3 oxidation state,[15] are compounds highly stabilized against oxidative phenomena (the main candidate in Pb replacement, i.e., Sn, easily oxidizes from +2 to +4, reducing the stability of the Sn-based OIHPs)[16] and nontoxic. Such replacement in OIHPs has been successfully investigated in combined theoretical/experimental works by Giustino, who demonstrated stability and applicability of these double perovskites in optoelectronics.[17] Still, Giustino et al.[18] have successfully synthesized $Cs_2AgBiCl_6$, characterizing its optical properties by means of photoluminescence (PL) measurements and optical absorption. The same group succeeded in synthesizing and characterizing $Cs_2AgBiBr_6$, showing the stability of such a compound and determining still by means of an experimental/theoretical approach the indirect gap of both bromine and chlorine compounds.[19] More recently, they finally characterized a similar class of compounds, Cs_2AgInX_6 (X = halide), and showed the tunability of their *direct* band gap as a function of the halide and demonstrated the possible formation of stable Cl/Br alloys.[20] The interest toward these double perovskites is further motivated by the encouraging results provided by this new architecture not only in PV but also in photocatalysis. Indeed, Zhou et al.[21] have shown the impressive stability in moisture and temperature of $Cs_2AgBiBr_6$ nanocrystals, making them extremely appealing for pollutant

Received: November 28, 2019
Accepted: January 2, 2020
Published: January 2, 2020

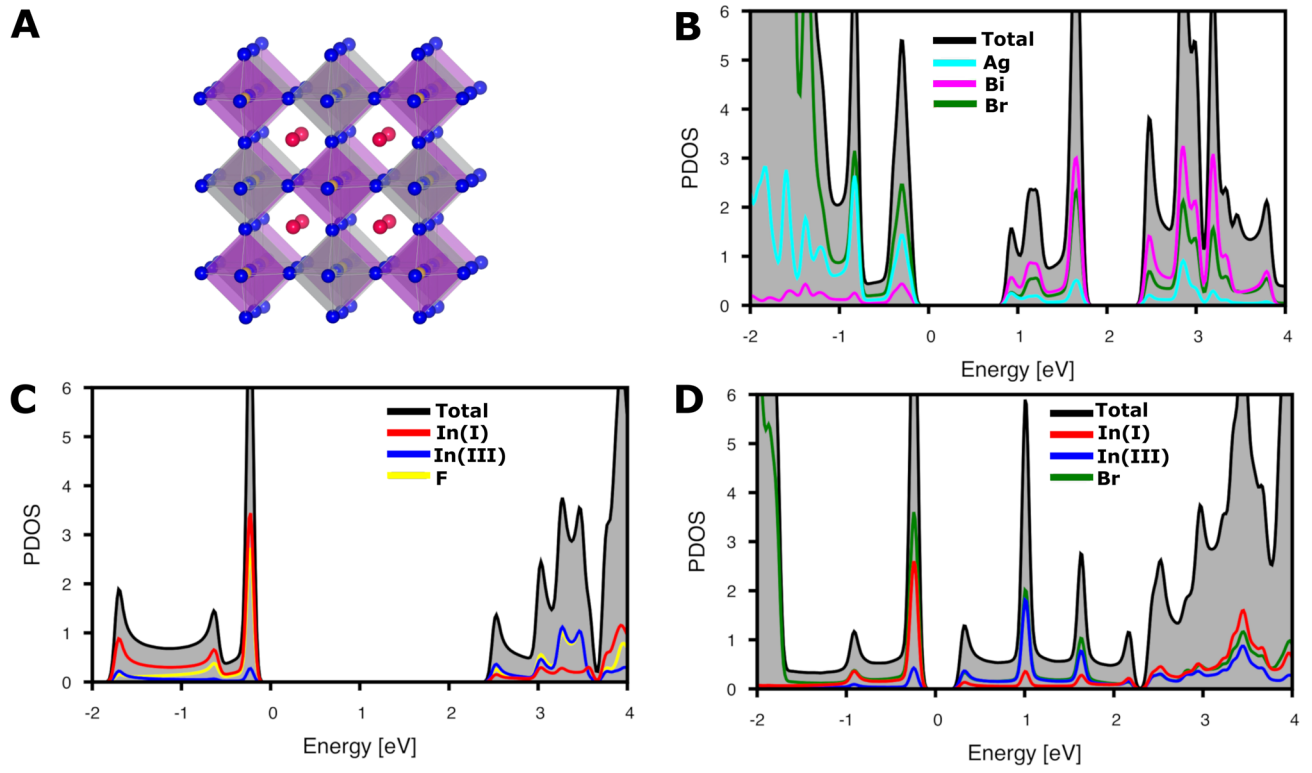

Figure 1. (A) Optimized structure of the $Cs_2AgBiBr_6$ crystal [red: Cs; gray: Ag; yellow: Bi; blue: Br]. DFT-PBE projected DOS of $Cs_2AgBiBr_6$ (B), $Cs_2In_2F_6$ (C), and $Cs_2In_2Br_6$ (D) including spin−orbit coupling (SOC).

reduction. Many others are the double-metallic lead-free perovskite compounds, both already synthesized and fully characterized and also hypothetical and not yet investigated.[22] Nevertheless, those based on Ag, Bi, and In elements remain undoubtedly the most promising for optoelectronics. Also, it is worth stressing that even if +3 is the most abundant In oxidation state, broad literature focusing on the +1 chemistry is similarly well-assessed.[23,24] Focusing more on the perovskite class of compounds, $CsInF_3$ and $CsInCl_3$ (not investigated here) have been theoretically predicted to show bond disproportion,[25] while very recently the synthesis of the tetragonal compound, nominally $Cs_{1.17}In_{0.81}Cl_3$, has confirmed the coexistence of the two oxidation states in the same compound.[26] Two related species, $CsTlX_3$ (X = F or Cl), have been synthesized, revealing an alternating pattern Tl(I)···Tl(III).[27] The same pattern has been observed in Au double perovskites,[28,29] where different Au−I bond lengths are clearly related with different oxidation states of gold atoms. Here, in view of their use in devices,[21,30] we aim to provide and discuss the main optoelectronic features of $Cs_2AgBiBr_6$, comparing them with those of $Cs_2In(I)In(III)X_6$ (X = F, Br),[31] another emerging class of compounds isostructural with $Cs_2AgBiBr_6$ (both characterized by the elpasolite structure). In particular, by means of state-of-the-art parameter-free ground- and excited-state calculations (for all of the details, see the SI), we compute the quasi-particle (QP) band structures, within the *GW* approach, and solve the Bethe−Salpeter equation (BSE) to obtain their optical properties. Our calculations clearly reveal the excitonic nature of the main optical peaks and—for the case of $Cs_2AgBiBr_6$—allow us to propose a new hypothesis concerning the nature of the observed PL spectrum and of the large measured Stokes shift. Indeed, while the main current interpretation relies on the multiphonon radiative recombination processes of free carriers, we show here that the position of the PL emission and the measured Stokes shift are fully compatible with the presence of direct and indirect bound excitons. Finally, from the accurate determination of the electronic and optical properties, we calculate the maximum theoretical photoconversion efficiency by using the SLME metrics[32] and compare the obtained values with those calculated for the other two perovskites of strong interest in PV applications: MAPI and $Cs_2Au_2I_6$ (see the SI for more details).

Figure 1 shows the optimized structure of $Cs_2AgBiBr_6$ discussed along the whole paper; as said, $Cs_2In_2X_6$ (X = F,Br) adopts a very similar structure of a cubic double perovskite (elpasolite). In $Cs_2AgBiBr_6$, the optimized lattice parameter of the primitive cell is a = 7.99 Å, while those of $Cs_2In_2Br_6$ and $Cs_2In_2F_6$ are 8.12 and 6.69 Å, respectively, results which are in good agreement with those in the literature.[19,33−35] In particular, for $Cs_2AgBiBr_6$, our result perfectly matches with the experimentally reported lattice parameter, which ranges between 7.92 and 7.96 Å. For the other two structures, octahedrally coordinated In(I) and In(III) atoms alternate: a shorter (longer) bond length implies a reduced (larger) oxidation state. For all of the species investigated here, we have calculated the density of states (DOS). As reported for other mixed quaternary perovskites, we here observe a different contribution of the B(I) and B(III) sites (B(I) = In(I), Ag; B(III) = In(III), Bi) to the projected DOS. In particular, for Br-based compounds, the valence band maximum (VBM) mainly consists of the orbital mixing of halide p orbitals and s orbitals of metals in the +1 oxidation state. A non-negligible contribution from s orbitals of metals in the +3 oxidation state is present around X (0.5, 0.0, 0.5) (it extends from X to W). For the fluorinated compound, at

https://dx.doi.org/10.1021/acsenergylett.9b02593
ACS Energy Lett. 2020, 5, 457−463

variance, the VBM consists of only In(I) and F orbitals, while +3 metallic orbitals are almost absent, revealing thus a more localized nature of the VBM. On the other hand, the conduction band minimum (CBM) is formed by the overlap of Bi, Br, and Ag (in decreasing amount) orbitals in $Cs_2AgBiBr_6$, with a similar trend that holds also in the case of In-based compounds, where In(III), Br/F, and In(I) (still in decreasing amount) orbitals form this band edge. As a general behavior, we observe that the DOS of the three materials shows sharper and narrow peaks near the VBM with respect to the CBM. Although the calculation of the electron−phonon scattering lifetimes is beyond the scope of the present work, from the above information about the DOS, we can state that the carrier nonradiative lifetime should be shorter for holes with respect to electrons: it is well known indeed that a smooth (narrow) DOS corresponds to a reduced (larger) number of carrier relaxation paths that lead to longer (shorter) carrier lifetimes.[7,36−38]

The DFT-PBE band structures of $Cs_2AgBiBr_6$ and of $Cs_2In_2X_6$ (X = F, Br) are reported in Figure S1 of the SI. They were obtained without and with the inclusion of the spin−orbit interaction, and our results are in essential agreement with the existing literature.[19] The corresponding QP band structures, with SOC included, are shown in Figure 2.

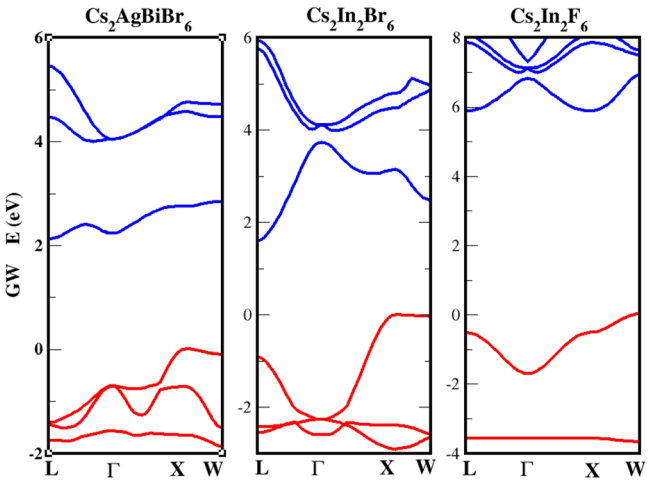

Figure 2. QP electronic band structures obtained within the *GW* perturbative approach; red (blue) indicates occupied (unoccupied) bands. The top of the valence band has been shifted to zero energy for all cases.

As expected, the role of the electronic correlation beyond the DFT-KS approach is to induce a large renormalization of the electronic gap with an opening of about 1.0 (0.7) eV for Br-based compounds and of 3.3 (3.0) eV for F-based compounds at the *GW* (G_0W_0) level of approximation (Figure S2 in the SI shows explicitly that the *GW* convergence for the case of $Cs_2AgBiBr_6$ is reached within three iterations). The three materials present an indirect character of the minimum electronic gap that does not change moving from Kohn−Sham (KS) (see Figure S1 in the SI) to QP scheme of calculation (red (blue) curves for occupied (unoccupied) states of Figure 2). The minimum indirect (direct) QP gaps are 2.1 (2.7) eV for $Cs_2AgBiBr_6$, 1.6 (2.5) eV for $Cs_2In_2Br_6$, and 5.9 (6.35) eV for $Cs_2In_2F_6$. Regarding $Cs_2AgBiBr_6$, it is worth mentioning that the band structure dispersion is very similar to the one reported by Giustino et al.,[19] although the QP gaps, calculated here at the *GW* level of approximation, are about 0.2 eV larger than those calculated at the G_0W_0 level of approximation. The large value of the direct and indirect electronic gap that we find here is not only in line with that obtained in ref 19 but also in reasonable agreement with the one found at the HSE06(+SOC) level of approximation in ref 39, where a value of 3.0 eV is reported for the direct one. Nevertheless, the same authors[39] do not include excitonic effects in the calculation of the absorption spectrum, obtaining an onset (similar to our IQP spectrum shown in Figure 3; see

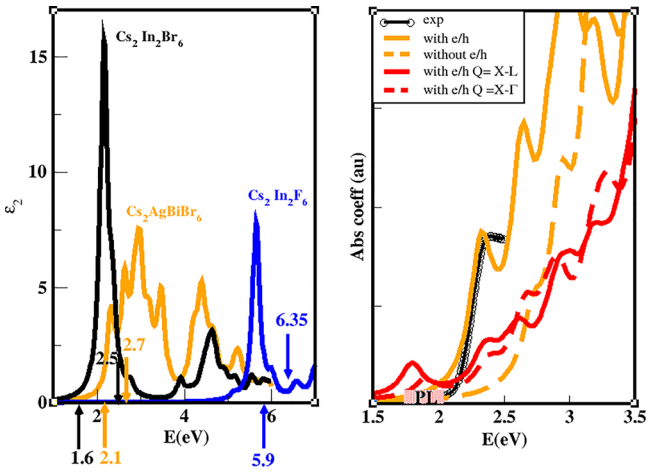

Figure 3. (Left) Imaginary part of the dielectric function for the three double perovskites, obtained taking into account the QP corrections calculated at the *GW* level of approximation and also including the excitonic and local-field effects through the solution of the BSE. The up-oriented (down) arrows (and relative numbers) indicate the energetic positions of the indirect (direct) minimum QP gap. (Right) Theoretical absorption coefficient with (orange solid curve) and without (orange dashed curve) the local field and excitonic effects, compared with the experimental curve (black curve) from ref 33. The red (dashed and solid) curves are the EELS spectra calculated with e−h effects included for finite transferred momentum Q corresponding to the lowest indirect transition L−X and Γ−X, respectively. The energetic region where the PL is observed is indicated schematically by the shaded yellow area.

discussion below) that results at too high energy with respect to the experimental one. For the sake of completeness, it is worth reporting the broad data available in the literature for both the direct and indirect electronic gap for $Cs_2AgBiBr_6$ at the HSE06+SOC level of calculation. Indeed, for the indirect one, the reported values range from 1.79 up to 2.18 eV.[40−44] More scarce is the availability of calculated direct gaps that range between 1.7 and 3 eV.[20,39,40]

We then move to show, in the left panel of Figure 3, the imaginary part of the dielectric function of the three double perovskites, obtained by solving the BSE. While $Cs_2AgBiBr_6$ has a broad spectrum (orange curve) in the vis/UV region, with the first peak at around 2.3 eV, a very intense optical peak at about 2.1 and 5.8 eV is present for $Cs_2In_2Br_6$ (black curve) and $Cs_2In_2F_6$ (blue curve), respectively. In the same figure, for each material, the values of the QP direct (indirect) gaps are indicated by up (down) arrows. It is then straightforward to extract the exciton binding energy (E^b_{exc}) of the first bright direct exciton (corresponding to the position of the first optical absorption peak), which is 0.34, 0.35, and 0.85 eV for

https://dx.doi.org/10.1021/acsenergylett.9b02593
ACS Energy Lett. 2020, 5, 457−463

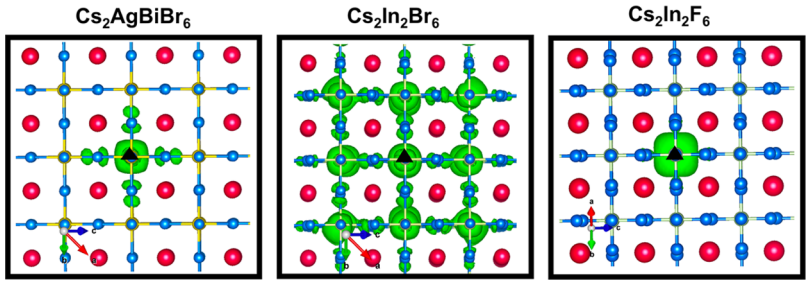

Figure 4. The green isosurface (15% of the maximum value) represents the probability of finding the electron when the hole is fixed in a given probable position (here shown as the black triangle). F atoms are blue dots; Br atoms are given in pale blue, Cs in red, In in pale yellow, Ag in pale green, and Bi in yellow.

$Cs_2AgBiBr_6$, Cs_2InBr_6, and $Cs_2In_2F_6$, respectively. In the first case (two latter), the lowest bright exciton is built up mainly by a mixing of IQP transitions near the X (W) point, between the VBM and CBM. From the analysis of the BSE eigenvalues, we find that several optically inactive excitons are present below the first bright one, with E^b_{exc} of the lowest energetic dark exciton at 0.48, 0.44, and 1.34 eV, respectively. Regarding the large values of E^b_{exc} obtained in the present work, it is important to point out which could be the role of the ionic contribution to the dielectric screening. Indeed, this is often considered as one of the main sources of the small excitonic binding energy in hybrid halide perovskites (see, e.g., refs 45−47). In a recent work,[48] Kresse and co-workers have shown (for $MAPbI_3$ and other hybrid halide perovskites) that when the exciton binding energy is much larger than the energy of the longitudinal optical (LO) phonon mode there is a negligible ionic contribution to the effective dielectric screening determining E^b_{exc}, which is then not lowered by ionic screening. Following a similar argument, being here $E^b_{exc} \gg \hbar\omega_{LO}$ (see the phonon DOS reported in Figure S3 in the SI), we can exclude, at least in ideal double perovskites with ordered atomic structures, that the ionic contribution plays a role in the exciton binding energy values. The right panel of Figure 3 illustrates the good comparison between the theoretical BSE (solid orange curve) and the experimental absorption spectrum (black circles, taken from ref 33) of $Cs_2AgBiBr_6$. The analysis of the BSE optical peaks reveals that the first three are mainly due to the mixing of direct optical transitions from VBM, VBM-1 to CBM, CBM +1 degenerate states around X, Γ, and near the middle of the Γ-X direction, respectively. Notably, the second peak involves also transitions from VBM-2 and VBM-3 bands. The corresponding theoretical spectrum calculated at the independent quasi-particle (IQP) level of approximation (orange dashed curve) is also reported to highlight again the importance of the inclusion of excitonic effects for a comparison with experimental data. It is worth mentioning that similar good agreement is also found with experimental data reported in refs 49 and 50, where the excitation spectrum shows a sharp decrease at about 2.7−2.8 eV, a feature present also in our BSE curve. Notably, we do not find evidence of the strong peak at 2.85 eV which is often attributed to the pure cubic phase and which instead is probably due to the Bi-rich yellow phase, as discussed in ref 49. As mentioned before, $Cs_2AgBiBr_6$ is characterized by a broad PL spectrum below 2 eV whose origin is still under debate: while several authors connect it to multiple phonon-assisted radiative interband recombination,[33,49] others relate it to the presence of spatially localized color centers.[50] Although ab initio calculations of phonon-assisted PL spectra have started to be available in the literature by means of nonequilibrium Greens functions plus finite-difference electron−phonon coupling,[51,52] here it would be prohibitive from a computational point of view due to the large unit cell. We focus then on the energy loss function $\Gamma(\mathbf{q}, \omega) \propto \mathrm{Im}\left(\frac{1}{\epsilon}(\mathbf{q}, \omega)\right)$ calculated at the $\mathbf{q}$ vectors of interest ($\mathbf{q}$ = L−X, Γ−X, red solid and dashed curves in Figure 3) and including the e−h interaction. This calculation can provide clear evidence of the presence of indirect bound excitons, allowing one to verify if their energy is in the same range of the observed PL emission. Indeed, assuming as the most probable process the one involving a single LO phonon and if this mode has a very small energy (as in the present case,[53] see also the SI), the PL spectrum should have the onset at the same energy of the lowest indirect excitons. Notably, the EELS spectra (red curves) show peaks below 2 eV, in the same energetic region of the observed PL (shaded yellow rectangle). This provides a strong indication of the fact that the PL is due to phonon-assisted radiative recombination of indirect bound excitons with $\mathbf{q}$ = L−X, Γ−X and energies 1.8, and 1.9 eV, respectively. From our analysis, we can conclude that the large measured Stokes shift is compatible with the energy difference between the direct and the indirect excitonic interband transitions. This result can in some way reconcile the inconsistency between the large Huang−Rhys factor S extracted from the measured Stokes shift and the not too large values of the Frölich constants $\alpha_e = 2.54$ and $\alpha_h = 2$ calculated recently by Steele et al.[49] Furthermore, the idea that bound excitons are at the origin of the observed PL is also compatible with the presence of spatially localized (see the discussion of Figure 4) states below the electronic gap, which have been experimentally identified in ref 50 but interpreted there as color centers. Finally, starting from the QP energies, the values of the Frölich constants reported above, and the energy of the LO mode, we estimate the energy shift due to the formation of large polarons from the mesoscopic Fröhlich model in a similar way to what was done in ref 48, obtaining a reduction of the QP gap of about 0.09 eV. This means that, although the polaronic state is less stable than the indirect bound excitons, part of the photoexcited direct excitons can decay there and then rapidly separate in space, never reaching the lowest indirect exciton bound state. Furthermore, charge separation after optical excitation can be favored by nonregularities in the electrostatic potential not taken into account in our simulations but realistically occurring in experimental samples. We are clearly aware that the role of atomic disorder, scattering, impurities, and multiphonon processes cannot be discarded, but the present analysis shows that the excitonic nature of the optical properties plays a crucial role for correct interpretation of the

https://dx.doi.org/10.1021/acsenergylett.9b02593
ACS Energy Lett. 2020, 5, 457−463

experimental data. To further characterize the excitonic properties of the three double perovskites, we show in Figure 4 the wave function modulus square of the first bright direct exciton.

For $Cs_2In_2F_6$ (right panel) fixing the hole near a F atom (black triangle), the electron localizes mainly near the first neighbor In atoms, as shown by the green isosurface (corresponding to 15%), showing a very strong spatial localization. An increase of the excitonic spatial delocalization is instead visible in the two plots of $Cs_2AgBiBr_6$ and $Cs_2In_2Br_6$, where the electron prefers to be near In sites when the hole position is fixed near a halogen atom (black triangle).

Due to the large absorption coefficients and gap in the visible region, $Cs_2AgBiBr_6$ is a material of interest for possible PV applications, and similarly, it should apply to $Cs_2In_2Br_6$. We then calculated the spectroscopic limited maximum efficiency (SLME)[54] that has been proved to be a good metric to determine the maximum efficiency that an absorber material can reach in a single-junction solar cell. It was derived by Yu and Zunger[32] within the thermodynamic detailed balance, but differently from the Shockley and Queisser (SQ) limit,[55] it considers the existence of various energetic sequences of direct (dipole-allowed and -forbidden) and indirect band gaps, the specific shape of the absorption near the threshold, and the dependence of nonradiative recombination losses on the energy separation between the minimum and the direct gap. The SLME calculation requires as input the standard solar spectrum, the absorption coefficient of the material, and also the values of the direct and indirect electronic gaps. The calculated SLME curves are almost constant for thicknesses larger than 1 μm, reaching the values reported in Table 1.

Table 1. Calculated SLME for the Three Double Perovskites[a]

material	SLME (%)
$Cs_2AgBiBr_6$	10.5
$Cs_2In_2Br_6$	11.5
$Cs_2In_2F_6$	0.1
MAPI	26
$Cs_2Au_2I_6$	30

[a]Values are compared with those obtained for MAPI and for $Cs_2Au(I)Au(III)I_6$.

Our theoretically predicted $Cs_2AgBiBr_6$ SLME is in good agreement with the previous theoretical one reported (7.92%@HSE06+SOC).[40] Comparing our value with experimentally reported PCEs for $Cs_2AgBiBr_6$, which are in the order of ~3%,[56−58] we predict large room for experimentally improving the light-harvesting performances for the two bromine-based materials. However, in single-junction solar cells based on ordered defect-free materials, the efficiency is likely not to reach the large values obtained by current OIHP-based devices. In this sense, our predicted SLME for MAPI (26.0%) is in good agreement with previous theory (24.94% @HSE06+SOC),[59] slightly larger, as expected, than the experimentally reported PCE values of 25.2%.[8] The value predicted for the $Cs_2Au_2I_6$, which is another Pb-free perovksite receiving increasing attention recently, confirms the high potential of this material for PV application, as suggested recently by Debicchi et al.[29] Finally, for $Cs_2In_2F_6$, due to the larger gap in the UV region, the calculated SLME is clearly very small.

In conclusion, by means of ground- and excited-state ab initio simulations, we here discussed and compared structural, electronic, and optical features of two classes of Pb-free double perovskites, i.e., stoichiometrically quaternary $Cs_2AgBiBr_6$ and ternary $Cs_2In_2X_6$ (X = F, Br). For the former, in particular, we observe that its first absorption peak is the result of a bound exciton close to the X point, while the PL spectrum is a phonon-assisted radiative recombination process of indirect bound excitons. Importantly, using our theoretical absorption coefficients and direct/indirect band gaps, we have calculated the spectroscopic limited maximum efficiency of these materials and observed a large room for enhancing their conversion efficiencies as light harvesters in devices.

■ ASSOCIATED CONTENT

Supporting Information

The Supporting Information is available free of charge at https://pubs.acs.org/doi/10.1021/acsenergylett.9b02593.

Theoretical details of DFT, *GW*, BSE, and spectroscopic limited maximum efficiency calculations and additional theoretical results that include the electronic band structure of $Cs_2AgBiBr_6$, $Cs_2In_2Br_6$, and $Cs_2In_2F_6$, total phonon DOS of the three species, convergence test of quasiparticles energies vs Kohn−Sham ones for $Cs_2AgBiBr_6$, and the convergence test of the optical spectra (BSE+G_0W_0) for the three species (PDF)

■ AUTHOR INFORMATION

Corresponding Authors

Maurizia Palummo − *University of Rome, Rome, Italy;* orcid.org/0000-0002-3097-8523; Email: maurizia.palummo@roma2.infn.it

Eduardo Berrios − *Universidad de Valparaíso, Valparaíso, Chile*; Email: eeduardo.berrios@uv.cl

Giacomo Giorgi − *The University of Perugia, Perugia, Italy, and CNR-ISTM, Perugia, Italy;* orcid.org/0000-0003-4892-7908; Email: giacomo.giorgi@unipg.it

Other Author

Daniele Varsano − *Istituto Nanoscienze-Consiglio Nazionale delle Ricerche (CNR-NANO), Modena, Italy;* orcid.org/0000-0001-7675-7374

Complete contact information is available at: https://pubs.acs.org/10.1021/acsenergylett.9b02593

Notes

The authors declare no competing financial interest.

#E-mail: daniele.varsano@nano.cnr.it.

■ ACKNOWLEDGMENTS

G.G., M.P., and D.V. acknowledge PRACE (G.G. is particularly grateful to Deconvolves project, Pra17_4466) and ISCRA-B and C initiatives for awarding access to computing resources on Marconi at CINECA, Italy. E.B. thanks FONDECYT 11171043 and PAI-CONICYT 79170125. M.P. acknowledges INFN for financial support through the National project Nemesys. G.G. is grateful to Dr. Masanori Kaneko (The University of Kyoto, Japan) for the useful suggestions for figure editing.

REFERENCES

(1) Kojima, A.; Teshima, K.; Shirai, Y.; Miyasaka, T. Organometal Halide Perovskites as Visible−Light Sensitizers for Photovoltaic Cells. *J. Am. Chem. Soc.* **2009**, *131*, 6050−6051.

(2) Stranks, S. D.; Eperon, G. E.; Grancini, G.; Menelaou, C.; Alcocer, M. J. P.; Leijtens, T.; Herz, L. M.; Petrozza, A.; Snaith, H. J. Electron−Hole Diffusion Lengths Exceeding 1 Micrometer in an Organometal Trihalide Perovskite Absorber. *Science* **2013**, *342*, 341−344.

(3) Xing, G.; Mathews, N.; Sun, S.; Lim, S. S.; Lam, Y. M.; Grätzel, M.; Mhaisalkar, S.; Sum, T. C. Long−Range Balanced Electron- and Hole−Transport Lengths in Organic−Inorganic $CH_3NH_3PbI_3$. *Science* **2013**, *342*, 344−347.

(4) Giorgi, G.; Fujisawa, J.-I.; Segawa, H.; Yamashita, K. Small Photocarrier Effective Masses Featuring Ambipolar Transport in Methylammonium Lead Iodide Perovskite: A Density Functional Analysis. *J. Phys. Chem. Lett.* **2013**, *4*, 4213−4216.

(5) Giorgi, G.; Fujisawa, J.-I.; Segawa, H.; Yamashita, K. Cation Role in Structural and Electronic Properties of 3D Organic-Inorganic Halide Perovskites: A DFT Analysis. *J. Phys. Chem. C* **2014**, *118*, 12176−12183.

(6) Giorgi, G.; Yamashita, K. Organic-inorganic halide perovskites: an ambipolar class of materials with enhanced photovoltaic performances. *J. Mater. Chem. A* **2015**, *3*, 8981−8991.

(7) Kawai, H.; Giorgi, G.; Marini, A.; Yamashita, K. The Mechanism of Slow Hot−Hole Cooling in Lead-Iodide Perovskite: First−Principles Calculation on Carrier Lifetime from Electron-Phonon Interaction. *Nano Lett.* **2015**, *15*, 3103−3108.

(8) *NREL Cell Efficiency Chart*. https://www.nrel.gov/pv/cell-efficiency.html (Accessed: Sept 6, 2019).

(9) Blancon, J.-C.; et al. Extremely efficient internal exciton dissociation through edge states in layered 2D perovskites. *Science* **2017**, *355*, 1288−1292.

(10) Giorgi, G.; Yamashita, K.; Palummo, M. Nature of the Electronic and Optical Excitations of Ruddlesden-Popper Hybrid Organic-Inorganic Perovskites: The Role of the Many−Body Interactions. *J. Phys. Chem. Lett.* **2018**, *9*, 5891−5896.

(11) Cao, D. H.; Stoumpos, C. C.; Farha, O. K.; Hupp, J. T.; Kanatzidis, M. G. 2D Homologous Perovskites as Light−Absorbing Materials for Solar Cell Applications. *J. Am. Chem. Soc.* **2015**, *137*, 7843−7850.

(12) Kagan, C. R.; Mitzi, D. B.; Dimitrakopoulos, C. D. Organic−Inorganic Hybrid Materials as Semiconducting Channels in Thin−Film Field-Effect Transistors. *Science* **1999**, *286*, 945−947.

(13) Weber, D. $CH_3NH_3PbX_3$, ein Pb(II)−System mit kubischer Perowskitstruktur/$CH_3NH_3PbX_3$, a Pb(II)−System with Cubic Perovskite Structure. *Z. Naturforsch., B: J. Chem. Sci.* **1978**, *33b*, 1443−1445.

(14) Kamat, P. V.; Bisquert, J.; Buriak, J. Lead-Free Perovskite Solar Cells. *ACS Energy Lett.* **2017**, *2*, 904−905.

(15) Giorgi, G.; Yamashita, K. Alternative, Lead-free, Hybrid Organic-Inorganic Perovskites for Solar Applications: A DFT Analysis. *Chem. Lett.* **2015**, *44*, 826−828.

(16) Ogomi, Y.; Morita, A.; Tsukamoto, S.; Saitho, T.; Fujikawa, N.; Shen, Q.; Toyoda, T.; Yoshino, K.; Pandey, S. S.; Ma, T.; Hayase, S. $CH_3NH_3Sn_xPb_{1-x}I_3$ Perovskite Solar Cells Covering up to 1060 nm. *J. Phys. Chem. Lett.* **2014**, *5*, 1004−1011.

(17) Giustino, F.; Snaith, H. J. Toward Lead-Free Perovskite Solar Cells. *ACS Energy Lett.* **2016**, *1*, 1233−1240.

(18) Volonakis, G.; Filip, M. R.; Haghighirad, A. A.; Sakai, N.; Wenger, B.; Snaith, H. J.; Giustino, F. Lead-Free Halide Double Perovskites via Heterovalent Substitution of Noble Metals. *J. Phys. Chem. Lett.* **2016**, *7*, 1254−1259.

(19) Filip, M. R.; Hillman, S.; Haghighirad, A. A.; Snaith, H. J.; Giustino, F. Band Gaps of the Lead-Free Halide Double Perovskites $Cs_2BiAgCl_6$ and $Cs_2BiAgBr_6$ from Theory and Experiment. *J. Phys. Chem. Lett.* **2016**, *7*, 2579−2585.

(20) Volonakis, G.; Haghighirad, A. A.; Milot, R. L.; Sio, W. H.; Filip, M. R.; Wenger, B.; Johnston, M. B.; Herz, L. M.; Snaith, H. J.; Giustino, F. $Cs_2InAgCl_6$: A New Lead-Free Halide Double Perovskite with Direct Band Gap. *J. Phys. Chem. Lett.* **2017**, *8*, 772−778.

(21) Zhou, L.; Xu, Y.-F.; Chen, B.-X.; Kuang, D.-B.; Su, C.-Y. Synthesis and Photocatalytic Application of Stable Lead-Free $Cs_2AgBiBr_6$ Perovskite Nanocrystals. *Small* **2018**, *14*, 1703762.

(22) Yin, H.; Xian, Y.; Zhang, Y.; Li, W.; Fan, J. Structurally Stabilizing and Environment Friendly Triggers: Double-Metallic Lead-Free Perovskites. *Sol. RRL* **2019**, *3*, 1900148.

(23) Tuck, D. G. The lower oxidation states of indium. *Chem. Soc. Rev.* **1993**, *22*, 269−276.

(24) Downs, A. J. *Chemistry of aluminium, gallium, indium, and thallium*; Blackie Academic & Professional: Glasgow, U.K., 1993.

(25) Kang, C.-J.; Kotliar, G. Material design of indium−based compounds: Possible candidates for charge, valence, and bond disproportionation and superconductivity. *Phys. Rev. Mater.* **2019**, *3*, 015001.

(26) Tan, X.; Stephens, P. W.; Hendrickx, M.; Hadermann, J.; Segre, C. U.; Croft, M.; Kang, C.-J.; Deng, Z.; Lapidus, S. H.; Kim, S. W.; Jin, C.; Kotliar, G.; Greenblatt, M. Tetragonal $Cs_{1.17}In_{0.81}Cl_3$: A Charge−Ordered Indium Halide Perovskite Derivative. *Chem. Mater.* **2019**, *31*, 1981−1989.

(27) Retuerto, M.; et al. Synthesis and Properties of Charge−Ordered Thallium Halide Perovskites, $CsTl_{0.5}^{+}Tl_{0.5}^{3+}X$ (X = F or Cl): Theoretical Precursors for Superconductivity? *Chem. Mater.* **2013**, *25*, 4071−4079.

(28) Giorgi, G.; Yamashita, K.; Palummo, M. Two−dimensional optical excitations in the mixed−valence $Cs_2Au_2I_6$ fully inorganic double perovskite. *J. Mater. Chem. C* **2018**, *6*, 10197−10201.

(29) Debbichi, L.; Lee, S.; Cho, H.; Rappe, A. M.; Hong, K.-H.; Jang, M. S.; Kim, H. Mixed Valence Perovskite $Cs_2Au_2I_6$: A Potential Material for Thin−Film Pb-Free Photovoltaic Cells with Ultrahigh Efficiency. *Adv. Mater.* **2018**, *30*, 1707001.

(30) Volonakis, G.; Giustino, F. Surface properties of lead-free halide double perovskites: Possible visible−light photo-catalysts for water splitting. *Appl. Phys. Lett.* **2018**, *112*, 243901.

(31) Filip, M. R.; Giustino, F. Computational Screening of Homovalent Lead Substitution in OrganicInorganic Halide Perovskites. *J. Phys. Chem. C* **2016**, *120*, 166−173.

(32) Yu, L.; Zunger, A. Identification of Potential Photovoltaic Absorbers Based on First−Principles Spectroscopic Screening of Materials. *Phys. Rev. Lett.* **2012**, *108*, 068701.

(33) Slavney, A. H.; Hu, T.; Lindenberg, A. M.; Karunadasa, H. I. A Bismuth−Halide Double Perovskite with Long Carrier Recombination Lifetime for Photovoltaic Applications. *J. Am. Chem. Soc.* **2016**, *138*, 2138−2141.

(34) Lozhkina, O.; Murashkina, A.; Elizarov, M.; Shilovskikh, V.; Zolotarev, A.; Kapitonov, Y. V.; Kevorkyants, R.; Emeline, A.; Miyasaka, T. Microstructural analysis and optical properties of the halide double perovskite $Cs_2BiAgBr_6$ single crystals. *Chem. Phys. Lett.* **2018**, *694*, 18−22.

(35) Wu, C.; Zhang, Q.; Liu, Y.; Luo, W.; Guo, X.; Huang, Z.; Ting, H.; Sun, W.; Zhong, X.; Wei, S.; Wang, S.; Chen, Z.; Xiao, L. The Dawn of Lead-Free Perovskite Solar Cell: Highly Stable Double Perovskite $Cs_2AgBiBr_6$ Film. *Adv. Sci.* **2018**, *5*, 1700759.

(36) Kubo, A.; Giorgi, G.; Yamashita, K. Anion Ordering in $CaTaO_2N$: Structural Impact on the Photocatalytic Activity. Insights from First-Principles. *Chem. Mater.* **2017**, *29*, 539−545.

(37) Bernardi, M.; Vigil-Fowler, D.; Lischner, J.; Neaton, J. B.; Louie, S. G. Ab Initio Study of Hot Carriers in the First Picosecond after Sunlight Absorption in Silicon. *Phys. Rev. Lett.* **2014**, *112*, 257402.

(38) Restrepo, O. D.; Varga, K.; Pantelides, S. T. First−principles calculations of electron mobilities in silicon: Phonon and Coulomb scattering. *Appl. Phys. Lett.* **2009**, *94*, 212103.

(39) Yang, J.; Zhang, P.; Wei, S.-H. Band Structure Engineering of $Cs_2AgBiBr_6$ Perovskite through Order-Disordered Transition: A First−Principle Study. *J. Phys. Chem. Lett.* **2018**, *9*, 31−35.

https://dx.doi.org/10.1021/acsenergylett.9b02593
ACS Energy Lett. 2020, 5, 457−463

(40) Savory, C. N.; Walsh, A.; Scanlon, D. O. Can Pb-Free Halide Double Perovskites Support High-Efficiency Solar Cells? *ACS Energy Letters* **2016**, *1*, 949−955.
(41) McClure, E. T.; Ball, M. R.; Windl, W.; Woodward, P. M. Cs_2AgBiX_6 (X = Br, Cl): New Visible Light Absorbing, Lead-Free Halide Perovskite Semiconductors. *Chem. Mater.* **2016**, *28*, 1348−1354.
(42) Du, K.-z.; Meng, W.; Wang, X.; Yan, Y.; Mitzi, D. B. Bandgap Engineering of Lead-Free Double Perovskite $Cs_2AgBiBr_6$ through Trivalent Metal Alloying. *Angew. Chem., Int. Ed.* **2017**, *56*, 8158−8162.
(43) Li, T.; Zhao, X.; Yang, D.; Du, M.-H.; Zhang, L. Intrinsic Defect Properties in Halide Double Perovskites for Optoelectronic Applications. *Phys. Rev. Appl.* **2018**, *10*, 041001.
(44) Xiao, Z.; Meng, W.; Wang, J.; Yan, Y. Thermodynamic Stability and Defect Chemistry of Bismuth-Based Lead-Free Double Perovskites. *ChemSusChem* **2016**, *9*, 2628−2633.
(45) Huang, L.-y.; Lambrecht, W. R. L. Electronic band structure, phonons, and exciton binding energies of halide perovskites $CsSnCl_3$, $CsSnBr_3$, and $CsSnI_3$. *Phys. Rev. B: Condens. Matter Mater. Phys.* **2013**, *88*, 165203.
(46) Even, J.; Pedesseau, L.; Katan, C. Analysis of Multivalley and Multibandgap Absorption and Enhancement of Free Carriers Related to Exciton Screening in Hybrid Perovskites. *J. Phys. Chem. C* **2014**, *118*, 11566−11572.
(47) Herz, L. M. How Lattice Dynamics Moderate the Electronic Properties of Metal-Halide Perovskites. *J. Phys. Chem. Lett.* **2018**, *9*, 6853−6863.
(48) Bokdam, M.; Sander, T.; Stroppa, A.; Picozzi, S.; Sarma, D. D.; Franchini, C.; Kresse, G. Role of Polar Phonons in the Photo Excited State of Metal Halide Perovskites. *Sci. Rep.* **2016**, *6*, 28618.
(49) Steele, J. A.; et al. Photophysical Pathways in Highly Sensitive $Cs_2AgBiBr_6$ Double-Perovskite Single−Crystal X-ray Detectors. *Adv. Mater.* **2018**, *30*, 1804450.
(50) Zelewski, S. J.; Urban, J. M.; Surrente, A.; Maude, D. K.; Kuc, A.; Schade, L.; Johnson, R. D.; Dollmann, M.; Nayak, P. K.; Snaith, H. J.; Radaelli, P.; Kudrawiec, R.; Nicholas, R. J.; Plochocka, P.; Baranowski, M. Revealing the nature of photoluminescence emission in the metal−halide double perovskite $Cs_2AgBiBr_6$. *J. Mater. Chem. C* **2019**, *7*, 8350−8356.
(51) Cannuccia, E.; Monserrat, B.; Attaccalite, C. Theory of phonon-assisted luminescence in solids: Application to hexagonal boron nitride. *Phys. Rev. B: Condens. Matter Mater. Phys.* **2019**, *99*, 081109.
(52) Paleari, F.; P. C. Miranda, H.; Molina-Sánchez, A.; Wirtz, L. Exciton−Phonon Coupling in the Ultraviolet Absorption and Emission Spectra of Bulk Hexagonal Boron Nitride. *Phys. Rev. Lett.* **2019**, *122*, 187401.
(53) Haque, E.; Hossain, M. A. Origin of ultra-low lattice thermal conductivity in Cs_2BiAgX_6 (X = Cl, Br) and its impact on thermoelectric performance. *J. Alloys Compd.* **2018**, *748*, 63−72.
(54) A Python3 implementation of the Spectroscopic Limited Maximum Efficiency (SLME) analysis of solar absorbers. https://github.com/ldwillia/SL3ME (Accessed Aug 30, 2019).
(55) Shockley, W.; Queisser, H. J. Detailed balance limit of efficiency of p−n junction solar cells. *J. Appl. Phys.* **1961**, *32*, 510−519.
(56) Greul, E.; Petrus, M.; Binek, A.; Docampo, P.; Bein, T. Highly stable, phase pure $Cs_2AgBiBr_6$ double perovskite thin films for optoelectronic applications. *J. Mater. Chem. A* **2017**, *5*, 19972−19981.
(57) Gao, W.; Ran, C.; Xi, J.; Jiao, B.; Zhang, W.; Wu, M.; Hou, X.; Wu, Z. High−Quality $Cs_2AgBiBr_6$ Double Perovskite Film for Lead-Free Inverted Planar Heterojunction Solar Cells with 2.2% Efficiency. *ChemPhysChem* **2018**, *19*, 1696−1700.
(58) Pantaler, M.; Cho, K. T.; Queloz, V. I. E.; Garcia Benito, I.; Fettkenhauer, C.; Anusca, I.; Nazeeruddin, M. K.; Lupascu, D. C.; Grancini, G. Hysteresis-Free Lead-Free Double-Perovskite Solar Cells by Interface Engineering. *ACS Energy Lett.* **2018**, *3*, 1781−1786.
(59) Kangsabanik, J.; Sugathan, V.; Yadav, A.; Yella, A.; Alam, A. Double perovskites overtaking the single perovskites: A set of new solar harvesting materials with much higher stability and efficiency. *Phys. Rev. Materials* **2018**, *2*, 055401.

https://dx.doi.org/10.1021/acsenergylett.9b02593
ACS Energy Lett. 2020, 5, 457−463